



# A Non-invasive Technique to Estimate the Onset of Creep Strength Deterioration

Minati Sahu and Sarmishtha Palit Sagar

Submitted: 6 July 2021 / Revised: 28 August 2021 / Accepted: 14 September 2021 / Published online: 7 October 2021

A material when exposed to high temperature under a constant load for a prolonged period, it experiences deformation due to Creep. The strength of precipitation hardening materials reduces when exposed to high temperature under load due to the coarsening of precipitates and their incoherency with the matrix. Growth of precipitates beyond a critical size introduces nonlinearity in the propagation of elastic waves through a material. This nonlinearity in the elastic waves can be measured by a parameter known as nonlinear ultrasonic (NLU) parameter which is proportional to the ratio of the amplitude of 2nd harmonic to the square of the amplitude of the fundamental frequency of the sinusoidal wave propagated through the material. This paper addresses the effect of generation and growth of precipitates and their sizes on the changes in NLU parameter in P92 steel, a prime candidate material for power plant, exposed at temperature 650 °C under a load of 120 MPa for a duration till the material ruptures due to creep. Two different mode of experiments under the same condition; multiple samples with single interruption (MSSI) and single sample with multiple interruptions (SSMI), were designed to establish NLU technique to assess the critical stage of the said material. It was observed that in both the test modes when the changes in the NLU parameter were plotted as a function of strain, the peak value of the NLU parameter corresponds to the onset of deterioration in the mechanical strength of the material. The results were verified through microstructural characterization and mechanical test.

**Keywords** creep, creep strength, microstructure, nonlinear ultrasonic, P92 steel, precipitation

## 1. Introduction

Creep, a critical factor in determining the structural integrity of power plant components, is a slow and progressive time dependent deformation process that occurs at high temperature on components subjected to mechanical loading. P92 steel, containing approximately 9Cr-0.5Mo-1.8W with minor additions of V, Nb, B and N is an attractive material for applications under such environments due to its superior creep resistance property along with good thermal conductivity, low thermal expansion and low manufacturing cost (Ref 1–5). Tempered martensitic lath structure, stabilized by the presence of different precipitates like  $M_{23}C_6$  ( $M = Cr, Fe$ ) carbides,  $MX$  carbonitrides ( $M = Nb, V; X = C, N$ ), is the cause of superior creep resistance in P92 steel (Ref 4–8). With longtime of exposure Laves phase precipitation takes place along the grain boundaries. The nucleation and growth of Laves phase diffuses tungsten from the matrix and weakens the effect of solid solution strengthening (Ref 6, 7). As a result, the mechanical strength of the material deteriorates. Hence, monitoring periodically the onset of generation and growth of Laves phase through some non-invasive technique can help to predict the remaining life of the component.

To date, creep damage monitoring of plant components is generally carried out using replica metallography (Ref 8, 9). Replica technique is informative only when void formation takes place prior to failure. Many research initiatives are there to monitor the progression of creep damage using different non-invasive techniques (Ref 10–18). Among them, in recent years, nonlinear ultrasonic (NLU) technique has been recognized as a promising approach to characterize microstructural damages in solids and fluids. This technique involves generation of higher harmonics of elastic wave of particular frequency when propagating through a material with nonlinear elastic behavior. Couple of studies have been made to find the applications of NLU for creep and fatigue damage evaluation (Ref 19–26).

Wang et al. (Ref 19) reported the application of NLU technique for characterizing the creep damage in ASME T92 steel welded joints. They observed an increase in NLU parameter in each part of the weld joints with increasing creep exposure time as compared to the un-exposed specimen and attributed this to the growth of creep cavities. Ohtani et al. (Ref 20) used this technique to evaluate creep damage in the heat-affected zone of Cr-Mo steel. They have also observed an increase in the amplitude of the second harmonic around the heat-affected zone due to the increase in the creep void density. Baby et al. (Ref 21) used titanium alloy for studying creep damage using the ultrasonic and NLU techniques. In their work it was found that as compared to the ultrasonic longitudinal wave velocity, NLU parameter is more sensitive to the damage accumulation. Valluri et al. (Ref 22) studied creep damage progression in 99.98% pure copper in continuous and interrupted mode of creep tests and measured static, second and third harmonic components of the incident signal. The peak value of NLU parameter was observed in the region of maximum void and the rupture occurred from the location corresponds to the maximum value of NLU parameter. Kim

Minati Sahu and Sarmishtha Palit Sagar, Advanced Materials and Processes Division, CSIR-National Metallurgical Laboratory, Jamshedpur 831 007, India. Contact e-mail: sarmi@nmlindia.org.

et al. (Ref 23) applied NLU technique to study creep damage in Ni-based super alloy using finite amplitude method. They observed that the increase in NLU parameter is due to the coarsening of the cuboidal  $\gamma'$  precipitates in the direction perpendicular to that of the applied stress and that there is an increase in the aspect ratio of  $\gamma'$  precipitates. Park et al. (Ref 24) investigated NLU response in aged and crept 9-12Cr steel. A concave shaped variation in NLU parameter with aging time was found. It was also observed that the value of NLU parameter is three times higher in the crept sample as compared to the aged sample. Though the literature studies show that many research studies were carried out to evaluate creep damage using NLU technique but not much information is available for its usefulness in assessing the critical stage of Cr-Mo steel (P92 steel used in this research). Moreover, no such detailed work has been carried out to establish the effect of precipitate size and volume fraction of precipitates on the change in NLU parameter. Above all, the studies on NLU (other than those from the authors research group) had been done either in pitch-catch or in through transmission mode. In Pitch-catch method, the transmitter and the receiver transducers are placed apart from each in the same line on one surface of the test material. This method is highly effective for surface damage assessment as the depth of penetration of elastic wave is restricted to few micron below the surface. Hence this method is not suitable for evaluating the damage status in the bulk. On the other hand, through transmission, where the transmitter and the receiver are placed perpendicularly on the two sides of the test material is effective for bulk property analysis but needs access to both the sides of a component which is generally impractical in industrial environment. To overcome these limitations of both the common NLU techniques, in this research work, we have used pulse-echo mode of NLU measurement. In the pulse-echo NLU (PENLU) technique, the transmitter and the receiver both are housed together and placed on one side of the material (Fig. 2). The elastic wave passes through the thickness of the material and reflects back from the other surface. The reflected signal is received by the receiver. Hence it is capable of capturing bulk information across the thickness of the material (creep is a bulk phenomenon) as well as requires only single side access of a component. To establish the applicability of the PENLU technique for creep progression evaluation, we have used two different mode of experiments; multiple samples with single interruption (MSSI) and single sample with multiple interruptions (SSMI). In MSSI mode, each sample was loaded and unloaded at a defined creep strain%. Interruptions for unloading were determined from the creep curve of the test material. Samples generated each with different strain% were used for NLU measurement, mechanical and microstructural characterization. In SSMI mode, a single sample was loaded for creep testing and unloaded at pre-defined strain% for NLU parameter measurement. This loading and unloading for creep testing and NLU parameter measurement of sample continues till the sample ruptured.

## 2. Origin of Ultrasonic Nonlinearity

Generation of higher harmonics is a classical phenomenon which occurs when an incident waveform is distorted due to nonlinear elastic response of the medium through which it

propagates (Ref 27). The nonlinear stress-strain relationship between stress and strain can be represented as follows:

$$\sigma = E\varepsilon(1 + \beta\varepsilon + \dots) \quad (\text{Eq 1})$$

where  $E$  is the Young's modulus,  $\beta$  is the second-order nonlinear elastic coefficient.

One dimensional ultrasonic wave equation can be expressed as (Ref 28–30):

$$\rho \frac{\partial^2 u}{\partial t^2} = \frac{\partial \sigma}{\partial x} \quad (\text{Eq 2})$$

where  $\rho$  is the density of the medium,  $u$  is the wave displacement,  $t$  is the time and  $x$  is the propagation distance of the wave.

The strain and the displacement are related as:

$$\varepsilon(x, t) = \frac{\partial u(x, t)}{\partial x} \quad (\text{Eq 3})$$

Ultrasonic wave Eq 2 in terms of strain can be written as:

$$\rho \frac{\partial^2 u}{\partial t^2} = E \left( \frac{\partial^2 u}{\partial x^2} + 2\beta \frac{\partial u}{\partial x} \frac{\partial^2 u}{\partial x^2} + \dots \right) \quad (\text{Eq 4})$$

The solution for the second-order Eq 4 can be obtained using the perturbation theory (Ref 30, 31). For this, the displacement 'u' is assumed as:

$$u = u_0 + u' \quad (\text{Eq 5})$$

where  $u_0$  and  $u'$  represent the initial wave and the first-order perturbation solution, respectively. If we assume  $u_0$  to be a sinusoidal wave of single frequency which is expressed as:

$$u_0 = A_1 \sin(kx - \omega t) \quad (\text{Eq 6})$$

Then the perturbation solution of Eq 4 up to the second order is as:

$$u = A_1 \sin(kx - \omega t) + \frac{\beta x k^2 A_1^2}{8} \cos(2kx - 2\omega t) + \dots \quad (\text{Eq 7})$$

where  $\omega (= 2\pi f)$  is the angular frequency of the wave at frequency  $f$ ,  $k (= \omega/c)$  is the wave number,  $A_1$  is the amplitude of the wave at the fundamental frequency. If the diffraction and the absorption effects can be neglected over the propagation distance  $x$ , a simple formula can be obtained for the quadratic nonlinear elastic parameter  $\beta$  as:

$$\beta = \frac{8A_2}{A_1^2 x k^2} \quad (\text{Eq 8})$$

where  $A_2$  is the displacement amplitude at twice the fundamental frequency.

## 3. Experimental

### 3.1 Material Used

P92 steel of composition Fe-0.1C-0.3Si-0.5Mn-9.0Cr-0.1Ni-0.6Mo-1.8W-0.2V-0.06Nb-0.05N-3.0Co-0.005B (all in wt.%) was used in this study. The as-received steel plate was normalized at 1075 °C for 1hr, cooled in air, and subsequently tempered at 775 °C for 3 hrs followed by air cooling. Flat samples with a gage length of 40 mm and a cross section of

10 mm × 5 mm were prepared for creep testing. Schematic diagram of sample with dimensional details used for testing is given in Fig. 1.

### 3.2 Creep Testing

Creep tests were performed on the tempered samples at temperature 650 °C and at a stress level of 120 MPa using standard creep testing machine (Make-Mayes; Model-TC 30). Two different ways of interrupted creep tests were designed:

[I] *Multiple Sample Single Interruption (MSSI)* In this mode, creep tests were carried out on different samples. Each sample was loaded for creep testing and unloaded at different strain%. Total 11 samples were prepared with strain% of 0.56, 0.82, 0.97, 1.5, 2.15, 2.61, 3.04, 3.99, 5.76, 8.19 and 10.25, respectively. The NLU parameter was measured for each crept sample and then the samples were used for microstructural analysis and mechanical property evaluation. Hence experiments carried out in MSSI mode generated microstructures and mechanical properties of a series of samples with different strain% along with corresponding value of NLU parameter. This has helped to understand the relationship between microstructural and mechanical properties with the variation of NLU parameter. The possibility of variation in nonlinearity parameter from sample to sample in the as-annealed condition was taken care by normalizing the measured NLU parameter with respect to the as-tempered value.

[II] *Single sample with multiple interruptions (SSMI)* In this test mode, a single sample was used for conducting creep test by interrupting at different creep strain. After each interruption, the sample was unloaded, the NLU parameter was measured at three different locations in the gage length of the sample and then the sample was again loaded for further creep testing until it ruptures. In SSMI mode, total 15 interruptions were made at creep strain (%) of 0.56, 0.82, 0.97, 1.56, 2.15, 2.61, 3.04, 3.51, 3.99, 4.6, 5.76, 6.23, 7.11, 8.19 and 10.25, respectively. Large number of interruptions are allowed to capture the NLU parameter for the entire creep curve with sufficient data in all the three stages of creep. Moreover, this test mode helped us to replicate periodic condition monitoring of any real industrial component susceptible to creep failure.

### 3.3 Mechanical Property Evaluation Using Ball Indentation (BI) Technique

The mechanical properties of crept samples were evaluated using the automated ball indentation (ABI) technique devel-

oped at CSIR-National Metallurgical Laboratory, Jamshedpur. ABI is a microprobe system for stress-strain behavior study (Ref 32, 33). In this technique, the amount of materials experiencing plastic deformation increases with each loading. As a result, yielding and strain hardening occur simultaneously. In our experiment, a tungsten carbide spherical indenter of 1.57 mm diameter was forced into the test specimen and the load–depth data were recorded. The applied load and depth of penetration were continuously monitored. For each loading cycle the total indentation depth ( $h_t$ ) was obtained corresponding to the maximum load and the plastic indentation depth ( $h_p$ ) was obtained after unloading was completed. Using the software, the slope of each unloading cycle was calculated. The intersection of this line with the zero load line determines the value of  $h_p$ . The parameters  $h_t$ ,  $h_p$  and the corresponding maximum loads were used for determining the mechanical properties; Ultimate tensile strength (UTS), yield strength (YS), strength co-efficient ( $K$ ), strain hardening exponent ( $n_h$ ) and true stress-true strain curve, etc (Ref 33).

### 3.4 Microstructural Analysis

The microstructural investigations were carried out on the tempered samples and on the longitudinal section of near grip and gage portion of the crept samples. FEG-scanning electron microscopy (SEM) and a JEOL transmission electron microscope (TEM) with an energy-dispersive x-ray spectroscope were used for microstructural study. SEM analysis were carried out for observing different types of precipitates and creep voids. For SEM imaging, after polishing samples were etched using Vilella's reagent (1gm picric acid +5ml HCl+100ml Ethanol). The secondary electron SEM images provided a clear microstructural morphology of the precipitates in samples. TEM foils were prepared by twin-jet electro polishing using a solution of 10% perchloric acid and 90% acetic acid. TEM analysis was carried out to observe the dislocation distribution as well as the precipitation morphology (for clear observation of MX type precipitates). The average size of precipitates and creep voids from the microstructure were determined using in-house developed image analysis software "MicrAn."

### 3.5 Pulse-Echo Nonlinear Ultrasonic (PENLU) Measurements

Nonlinear ultrasonic measurements were carried out in Pulse-Echo mode using a specially fabricated probe mounting both 5 MHz crystal as a transmitter ( $T$ ) and 10 MHz crystal as a receiver ( $R$ ) in the same housing. The crystals were housed in a

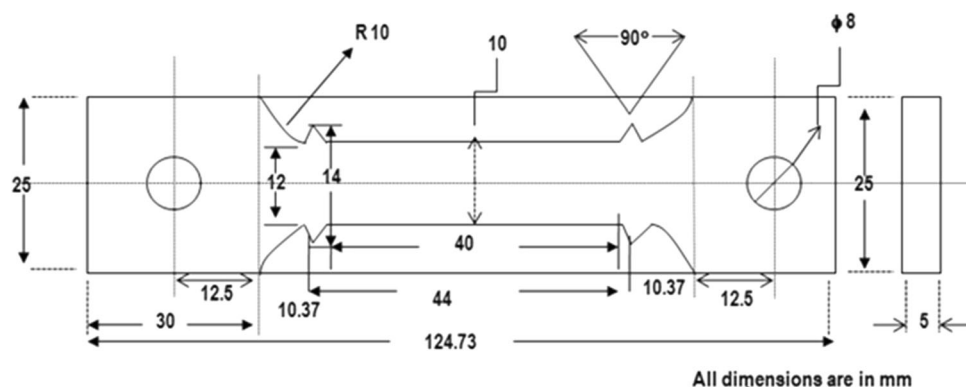


Fig. 1 P92 steel sample used for creep testing (all dimensions are in mm)

way so that the wave focused at a depth equal to the thickness of the test material. In our experiment, focal length was 5 mm. A schematic of the experimental setup along with the test sample is shown in Fig. 2. A fixture for holding the probe was fabricated to assure constant load between the transducer and the sample. The transducer was coupled to the sample with a thin layer of oil.

A five-cycle tone burst Hanning windowed signal generated by a PXI-based high power pulser (Ultra $\beta$ ) was used for exciting the transmitter. The signal received by the 10MHz crystal was filtered and analyzed in the frequency domain to extract the amplitudes of fundamental ( $A_1$ ) and the second harmonic ( $A_2$ ). A typical received signal and its spectral components are shown in Fig. 3(a) and (b), respectively.

All the analysis from the FFT of the received signal for the determination of NLU parameter which is defined in Eq 8 were done using in-house developed software Cal $\beta$ <sup>®</sup>. The software is having a calibration module for rejecting any spurious signal along with averaging large number of measurements. This special option takes care of the scatter in NLU measurement which is an obvious disadvantage of the NLU technique. The relative change in the NLU parameter ( $\beta_{rel}$ ) with respect to the value obtained before creep testing ( $\beta_o$ ) was considered as the measurement parameter and is defined as:

$$\beta_{Rel} = \frac{(\beta_{cr} - \beta_o)}{\beta_o}, \quad (\text{Eq 9})$$

where  $\beta_{cr}$  is the measured value of NLU parameter after creep. NLU measurements were carried out at three different locations in the gage section of the test samples. All the measurements were taken perpendicular to the creep loading direction. Averaging of the measurement data was made by taking five measurements at each location on every sample.

## 4. Results and Discussion

### 4.1 Creep Behavior

Figure 4 shows the creep curve, i.e., creep strain vs. time as obtained at a temperature of 650 °C under stress of 120MPa. Three distinctive regions of creep i.e., primary transient stage (Stage I~Strain 1%), secondary steady stage (Stage II~strain 6%) and accelerated tertiary stage (Stage III: Strain beyond 6% up to ~ 11%) which leads to failure of the material were observed.

### 4.2 Nonlinear Ultrasonic

Results of Nonlinear ultrasonic measurement in MSSI and SSMI modes are presented in this section.

**4.2.1 Interrupted Creep Tests.** *4.2.1.1 Single Sample Multiple Interruptions (SSMI).* The variation of relative NLU parameter ( $\beta_{rel}$ ) with strain (%) at three different measurement points in the gage length in SSMI mode is presented in Fig. 5. There is a small increase in  $\beta$  till strain around 1% (at the transition from stage I to II) after which there is no such change in  $\beta$ . Thereafter, a significant increase in  $\beta$  till 6% strain followed by a drop. It was also observed that the value of NLU parameter,  $\beta$  was significantly higher at the location 3 compared to other two locations from 4% of strain onward. This indicates that the damage accumulation is higher at the location 3. The test sample is ruptured from that very location only.

*4.2.1.2 Multiple Samples with Single Interruptions (MSSI).* Figure 6 shows the variation of relative NLU parameter ( $\beta_{rel}$ ) with creep strain in the MSSI mode. It is observed that the nature of the variation of NLU parameter is same as observed in the SSMI mode. There is an increase in the NLU

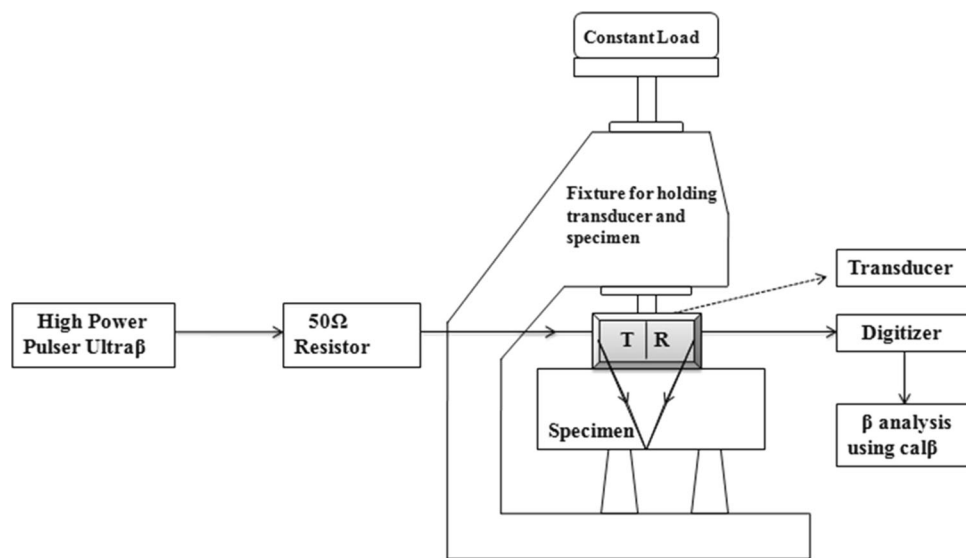
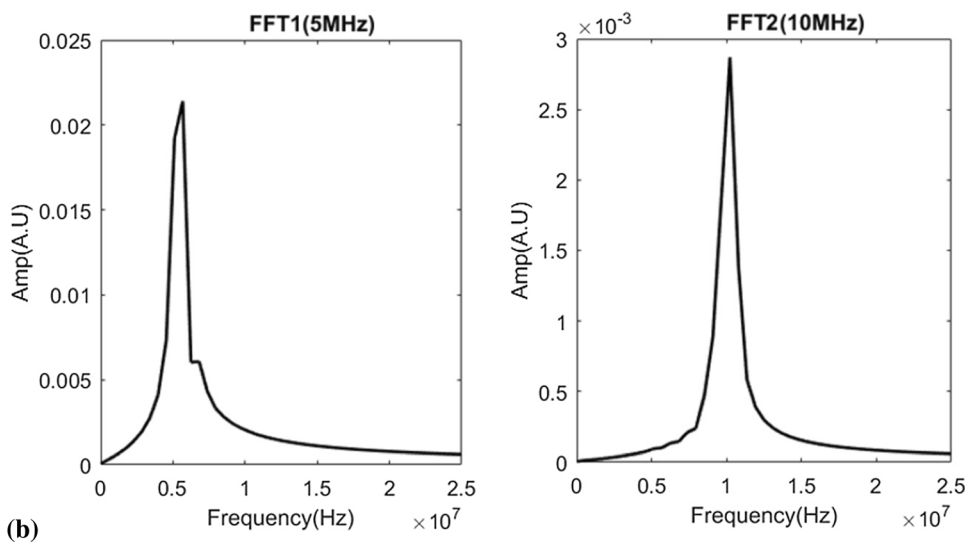
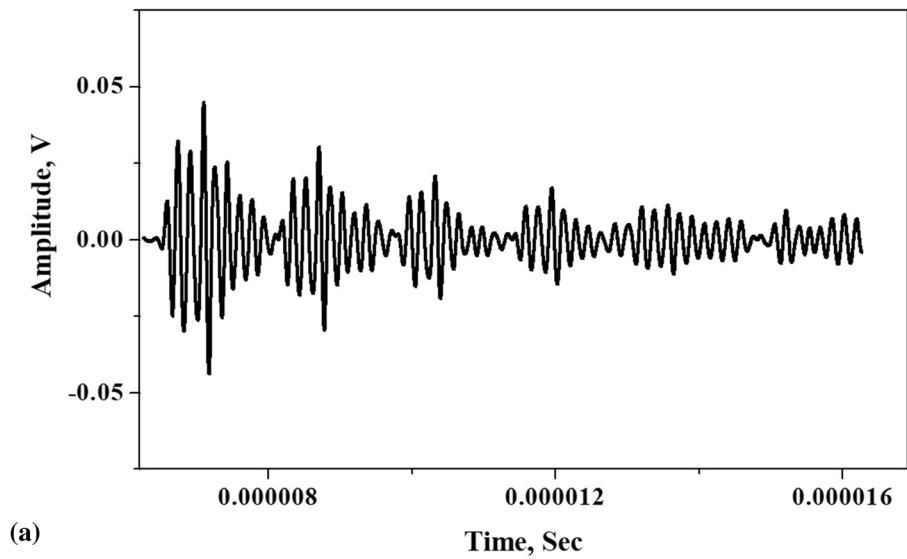
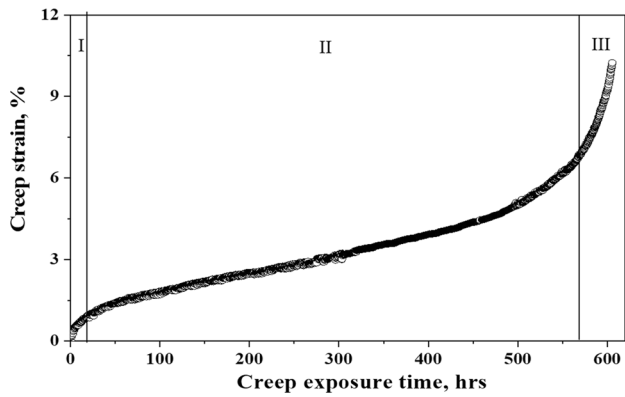


Fig. 2 Block diagram of experimental set up for measuring the nonlinear ultrasonic parameter



**Fig. 3** (a) Typical received signal in time domain. (b) Fourier spectrum of the 1st received signal showing the amplitudes of the fundamental and second harmonics used to determine NLU parameter



**Fig. 4** Creep strain vs. time curve for P92 steel at temperature of 650 °C and 120 MPa

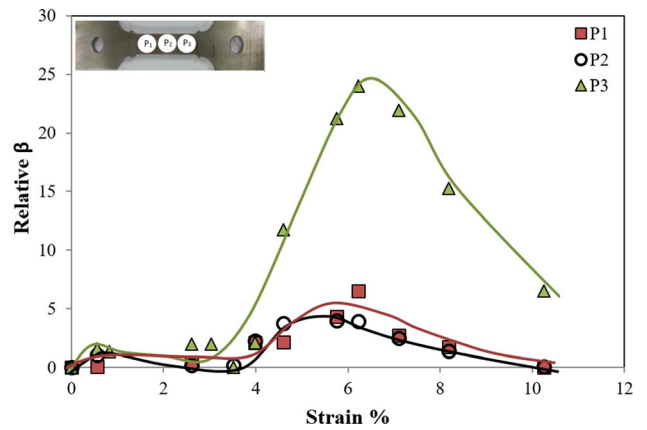


**Fig. 5** Variation of relative change in  $\beta$  ( $\beta_{rel}$ ) in three different measured positions with strain% in SSMI mode (Inset: Sample along with measurement positions)

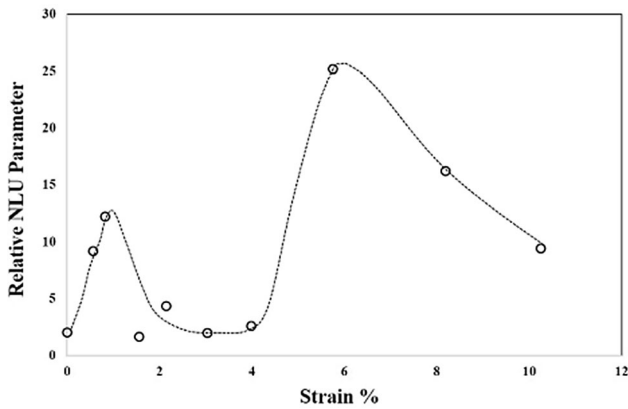


**Fig. 6** Variation of relative change in  $\beta$  ( $\beta_{rel}$ ) with Strain% in MSSSI mode

parameter till 1% of strain followed by a plateau and then a drastic increase till 6% of strain after which it drops. Attempts were made to understand the variation of NLU parameter with creep strain% through microstructural evolution with creep progression using the samples generated in MSSSI mode.

### 4.3 Microstructural Evolution

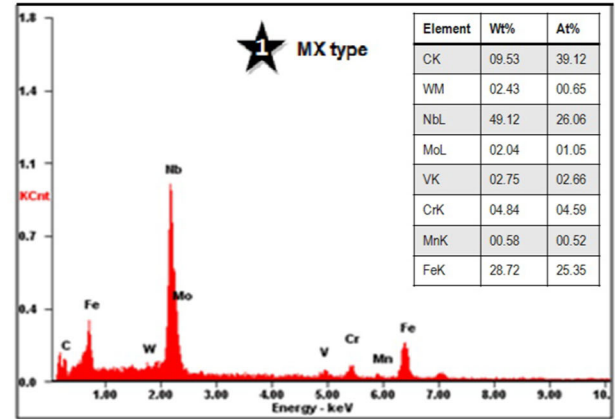
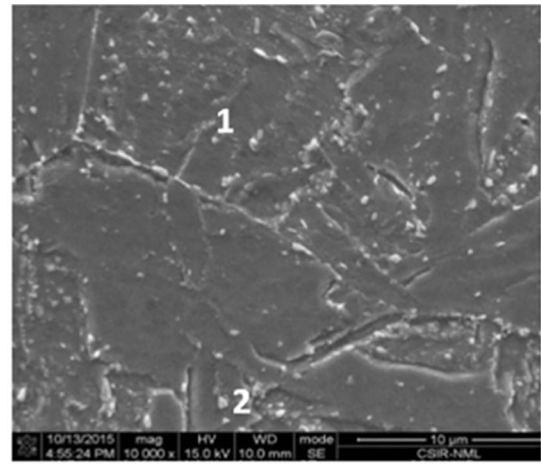
The microstructure along with EDAX analysis of as-tempered sample (Fig. 7) revealed martensitic structure with lath blocks and pockets in the grain. The grain boundaries are populated with  $M_{23}C_6$  type particles (specially  $M = Cr$ ) of average size around 100 nm and the interiors are filled with MX type ( $M = Nb$  and  $V$ ;  $X = N$  and  $C$ ) precipitates of average size approximately 30 nm.

SEM micrographs of gage section of samples at creep strain of 0.5, 1, 4, 6, 8 and 10.25% are shown in Fig. 8. It was observed from the micrographs that with increase in strain%, there was an increase in the grain size, coarsening of precipitates followed by micro-void formation at 8% strain and beyond.

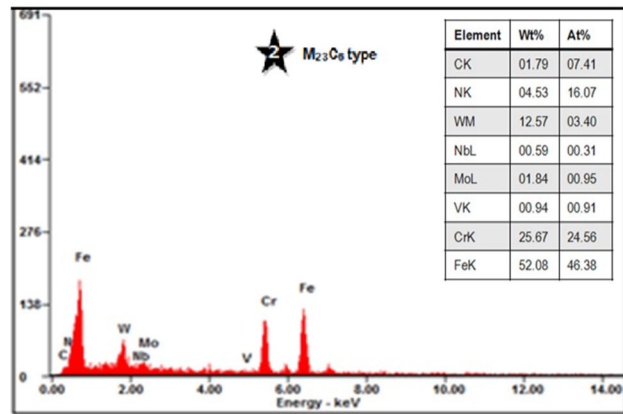
Transmission electron microscopy (TEM) was also carried out to further understand microstructural evolution. Figure 9 shows the TEM images of as-tempered and crept samples. The typical microstructure of P92 steel is tempered martensite composed of martensite laths with high dislocation density and precipitates distributed along the grain boundaries and the lath boundaries. The normalization treatment leads to a martensite matrix and precipitates such as  $M_{23}C_6$  ( $M = Cr, Fe$ ) carbides and MX ( $M = V, Nb, Ta$  and  $X = C, N$ ) carbonitrides along the boundaries. The tempered martensite is a homogeneous single phase with a good combination of high strength and high toughness.

In the crept samples, along with  $M_{23}C_6$  and MX precipitates, Laves phases were observed. The chemical compositions of all the precipitates and the matrix were confirmed by energy-dispersive x-ray spectroscopy (EDS) and are shown in Fig. 10(a), (b), (c) and (d).

Size quantification of different types of precipitates as observed in the TEM micrographs at different creep strain were done using the developed “MicrAn” software. Figure 11 depicts the change in the precipitate size with creep strain%. A gradual increase in the size of  $M_{23}C_6$  precipitates and Laves phase particles was observed with the increase in creep strain. The observed average size of  $M_{23}C_6$  precipitates at 1%, 6% and



(a)



(b)

**Fig. 7** SEM micrograph along with elemental analysis of (a) MX type (Niobium carbide) (b)  $M_{23}C_6$  type (Chromium carbide) precipitate of as-tempered sample

10.25% of creep strain was approximately 100 nm, 150 nm and around 250 nm, respectively, and the size of Laves phase at 1%, 6% and 10.25% creep strain was approximately 170 nm, 300 nm and 550 nm, respectively. The coarsening behavior of MX type precipitates was relatively slow achieving at size around ~ 50 nm at 10.25% of strain.

To understand the effect of precipitate size irrespective of the type of precipitates, classifications into four categories, finer (up to 40 nm), fine (41-50 nm), coarse (151-300 nm) and coarser (301 nm- above) were made based on the precipitates

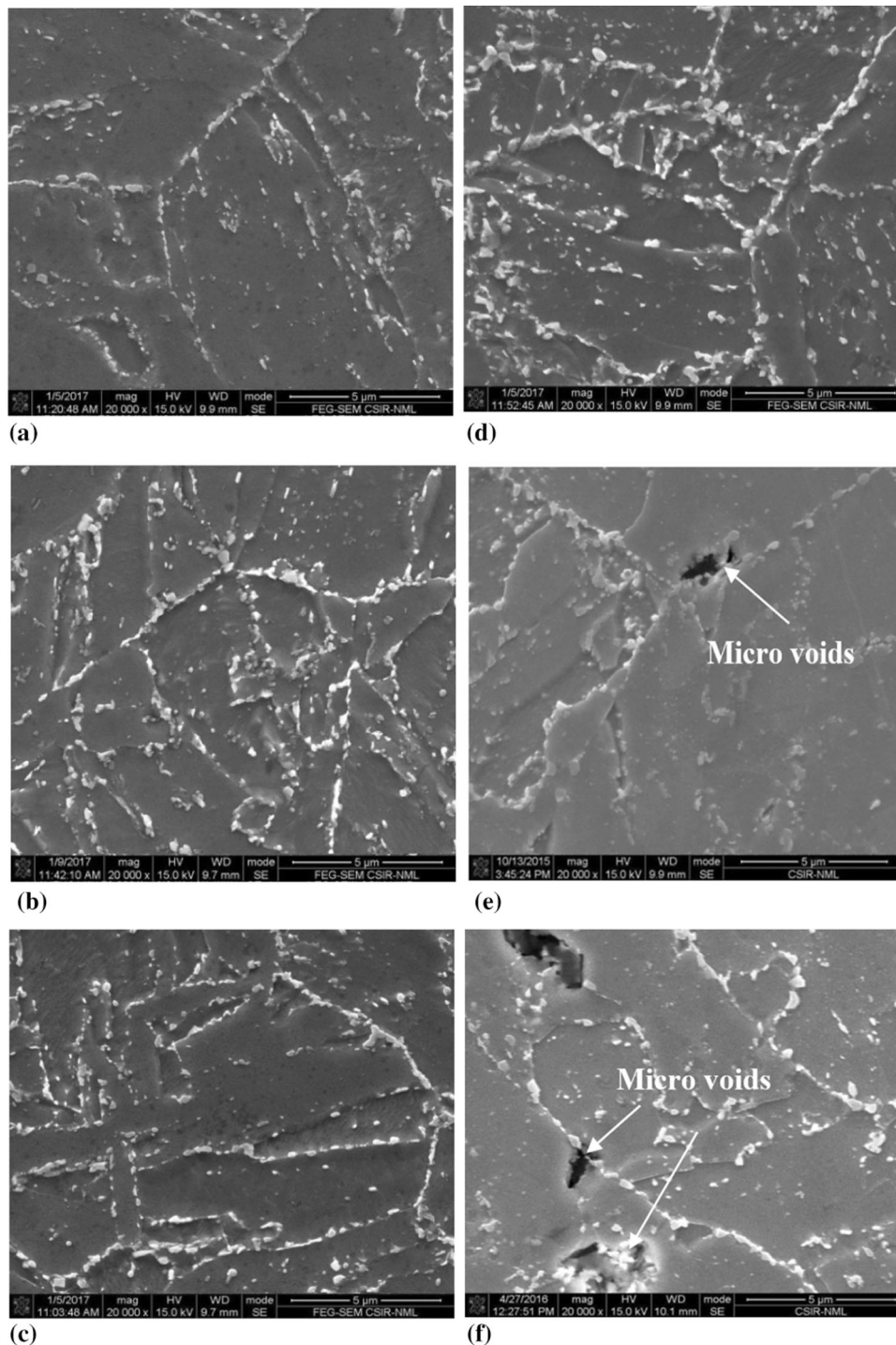


**Fig. 8** (a-f) SEM micrographs at strain of (a) 0.5%, (b) 1%, (c) 4%, (d) 6%, (e) 8%, (f)10.25% of samples creep tested in MSSSI mode

mean size. The ranges were selected from the growth kinetics of all three types of precipitates at different strains as shown in Fig. 11. This exercise was carried out to establish the effect of precipitate size and area fraction on the change in NLU parameter. The % of the area fraction of each category of precipitates was determined from the ratio of the total area of the precipitates to the image size. The calculated area fraction

of precipitates in crept sample at different creep strain is depicted in the bar graph in Fig. 12. Averaging of precipitate size was done using five micrographs at each strain.

It is clearly observed from the above bar graph that the total area fraction of precipitates are increasing with strain% and the nature of variation is very similar to the variation of NLU parameter (Fig. 6).

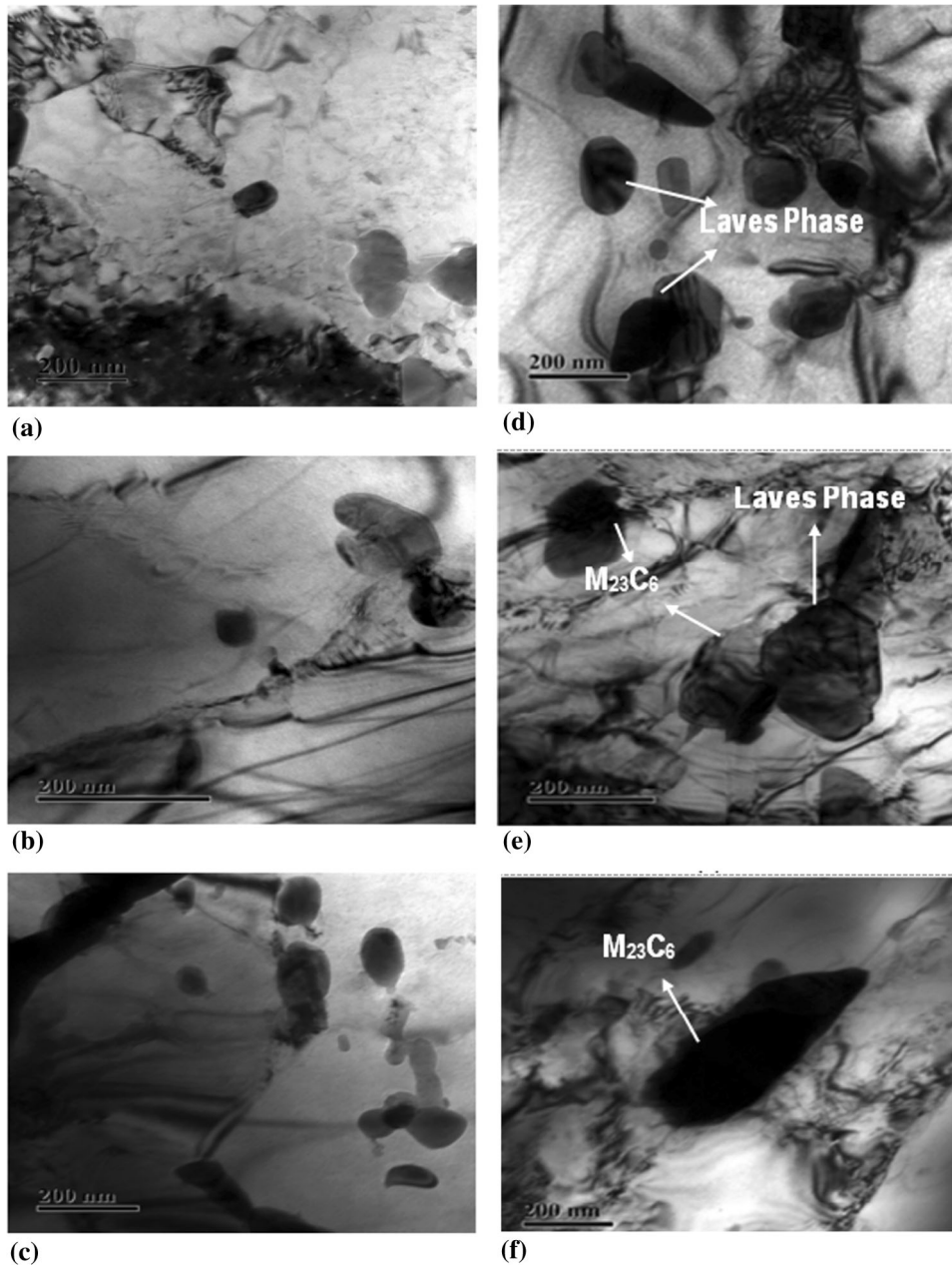


**Fig. 9** TEM micrographs at strain of (a) 0.5%, (b) 1%, (c) 4%, (d) 6%, (e) 8%, (f) 10.25%

#### 4.4 Mechanical Properties Evaluation

Load vs. depth and true stress vs. true plastic strain curves as obtained from ABI tests are shown in Fig. 13(a) and (b) respectively.

From the load-depth curve, the total indentation depth ( $h_t$ ) and the plastic indentation depth ( $h_p$ ) were calculated and used to evaluate the strain hardening exponent ( $n_h$ ) and strength coefficient ( $k$ ) of the crept sample for different creep strain% (Ref 33, 34).

Further, for determining  $k$  and  $n_h$  values, regression analysis using a power law equation was carried out for different values of  $\sigma$  and  $\epsilon_p$  (Ref 33):

$$\sigma = k\epsilon_p^{n_h} \quad (\text{Eq 10})$$

where  $\sigma$  is the true stress and  $\epsilon_p$  is the true plastic strain. For calculating these values, indentation diameter and load data points were used and are given by the following equation:

$$\epsilon_p = k_1 \frac{d_p}{D} \quad (\text{Eq 11})$$

and

$$\sigma = 4 \cdot P / \pi \cdot d_p^2 \delta' \quad (\text{Eq 12})$$

where  $P$  = applied load,  $d_p$  = plastic indented diameter,  $D$  = diameter of the indenting ball and  $\delta'$  is a constraint factor.

Figure 14 depicts the variation of the strain hardening exponent ( $n_h$ ) and the strength coefficient ( $k$ ) with creep strain. A drop in the strength coefficient as well as in the strain hardening coefficient was observed after 6% strain.



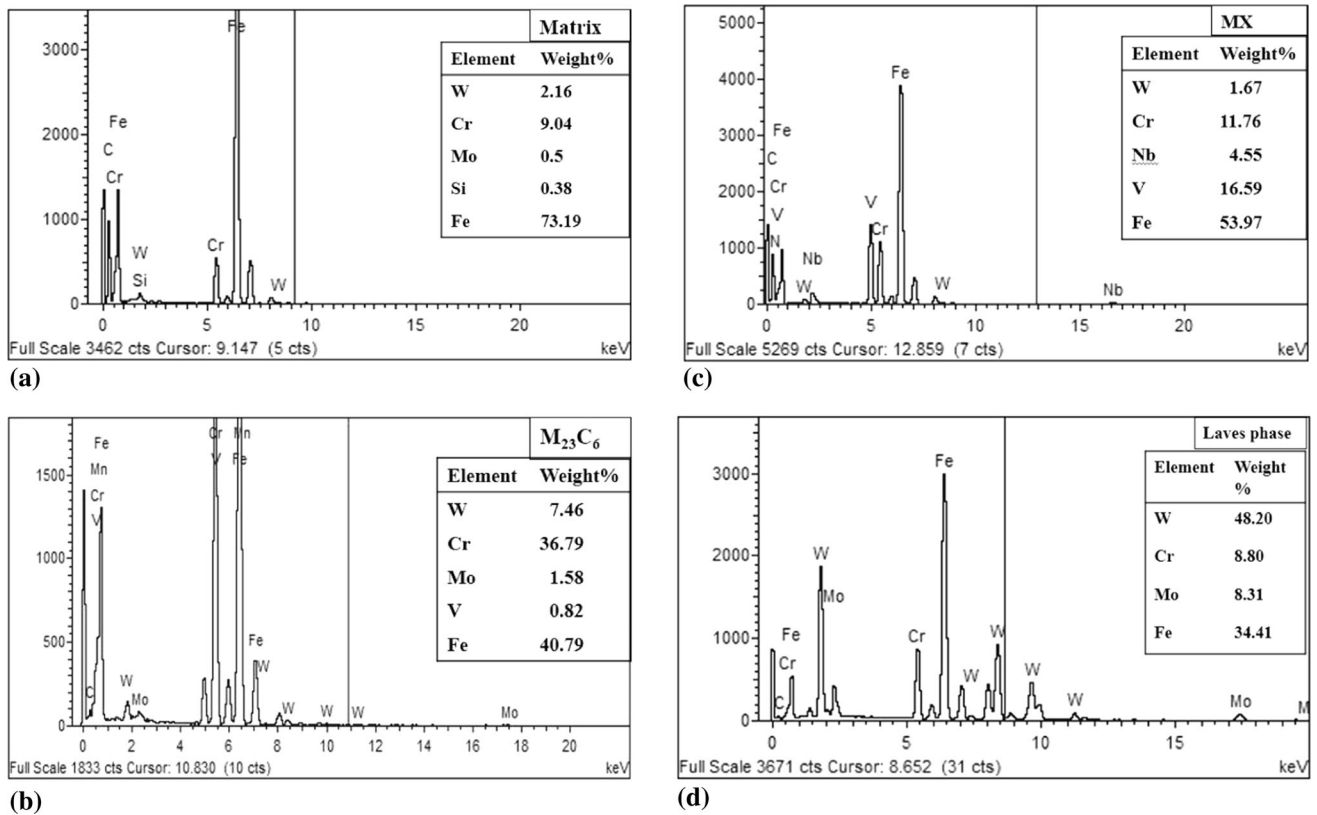


Fig. 10 EDAX analysis of different precipitates (a) Matrix, (b)  $M_{23}C_6$  (c) MX and (d) Laves phase

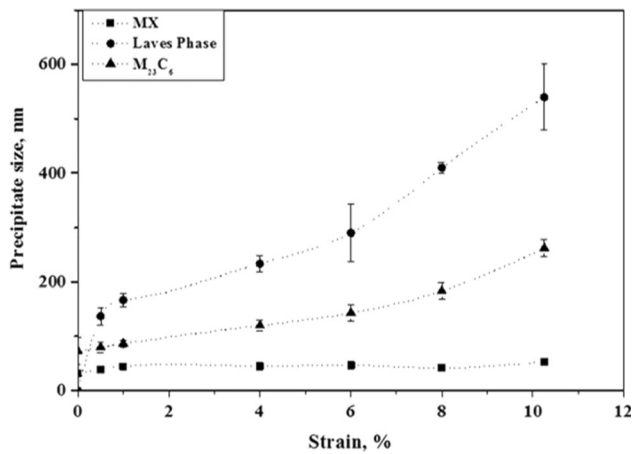


Fig. 11 Mean size of different precipitates at different creep strain% as determined from TEM micrographs

## 5. Discussion

Results of nonlinear ultrasonic measurements in both the test modes, MSSSI and SSMI, showed the same trend in the variation of NLU parameter. The variation of NLU parameter with strain follows the creep curve of the material as shown in Fig. 4. The entire graph of NLU parameter variation with strain can also be divided into three different regions: Region I (up to ~1% strain); in this region, there is a slight increase in  $\beta$ , Region II (from 1 to 6% strain); region with a significant increase in NLU parameter and Region III (after 6% strain till specimen rupture); Drop in NLU parameter.

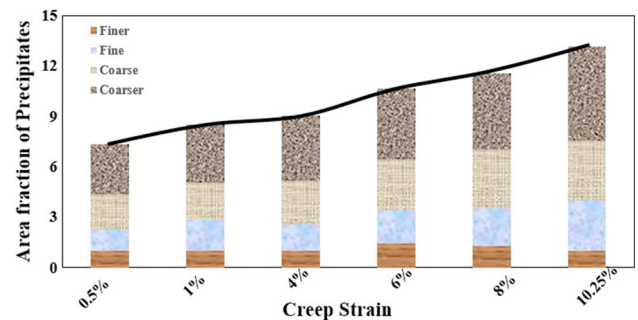
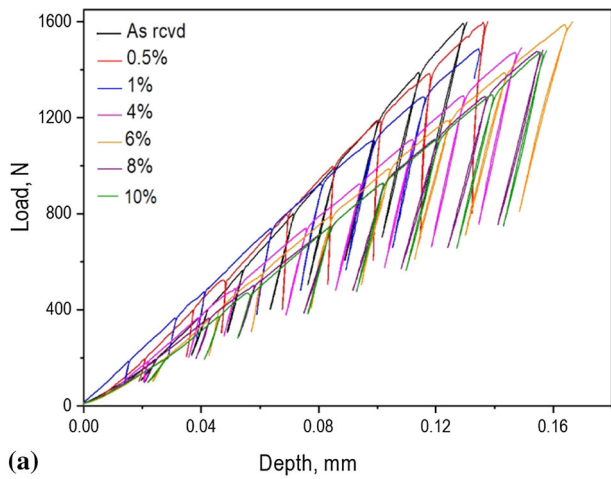
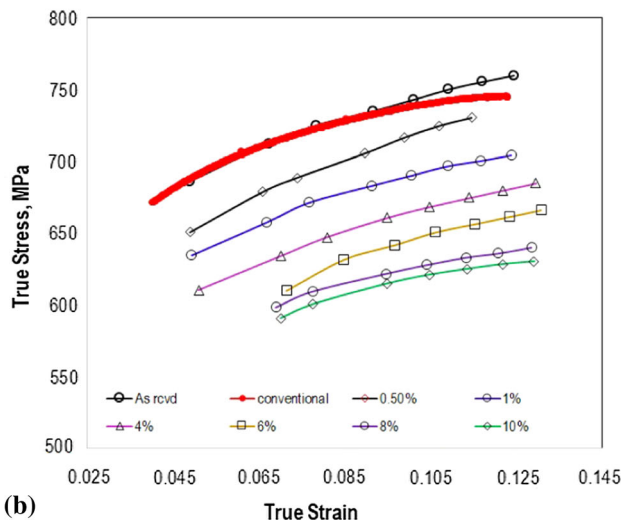


Fig. 12 Area fraction of different types (finer, fine, coarse and coarser type) of precipitates at different strain%

It has been established by many researchers that the NLU parameter is strongly dependent on the stress and the dislocation density and the relationship is expressed as  $\beta \propto NL^4\sigma$ , where  $N$  = dislocation density;  $L$  = dislocation loop length and  $\sigma$  is the applied/ residual stress (Ref 5, 35). It has also been discussed in a few theoretical studies (Ref 23, 29–31) that a sinusoidal elastic wave is distorted significantly by the presence of precipitates. The size of precipitates is much smaller than the wavelength of the elastic wave which will cause scattering of ultrasonic waves. Hence as the size of precipitates increases, it results in the distortion of the wave propagation. Moreover, the precipitate has lattice spacing different from that of the matrix. When the second phase precipitates are within the coherency limit, the precipitate matrix interface is strong as the misfit is small. With increase in the size of precipitates, lattice strain



(a) Load vs. Depth curve



(b) True stress vs. true strain curve

**Fig. 13** (a) Load vs. Depth curve, (b) True stress vs. true strain curve of P92 creep samples for different strain%

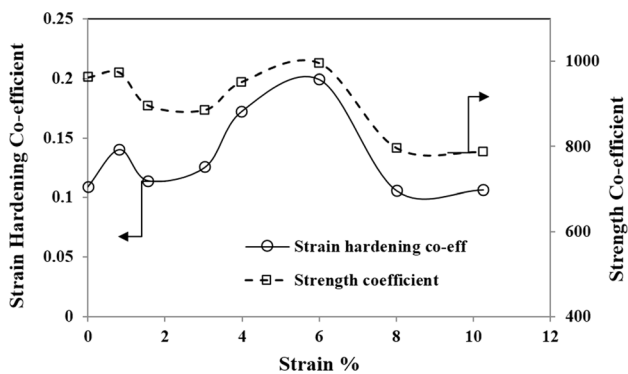


**Fig. 14** Variation of strain hardening coefficient and strength coefficient with strain%

risers because of the mismatch between the second phase and the matrix, which can be measured by a misfit parameter,  $\delta$ , as:

$$\delta = \frac{2(a_p - a_m)}{(a_p + a_m)} \quad (\text{Eq 13})$$

where  $a$  and  $a_m$  are lattice parameters of the precipitates and the matrix.

It was shown by Norris (Ref 28) and Cantrell (Ref 30) that for spherical and elastically isotropic precipitates, the coherency strain ( $\varepsilon$ ) generated in the matrix due to the misfit is given by (Ref 28):

$$\varepsilon = \frac{3K\delta}{3K + 2E(1 + \nu)} \quad (\text{Eq 14})$$

where  $K$  is the bulk modulus of the precipitate,  $E$  and  $\nu$  are the Young's modulus and Poisson's ratio of the matrix. This strain field resulted from the mismatch of the second phase particle and the matrix may increase the stress (Ref 28–30). The increase in the stress due to the coherency strain is given by

$$\Delta\sigma \cong 6\mu \left(\frac{r_a}{b}\right)^{1/2} V_f^{1/2} \varepsilon^{3/2} \quad (\text{Eq 15})$$

where  $V_f$  is the volume fraction of the dispersed phase and  $r_a$  is the precipitate radius and  $\varepsilon$  is the coherency strain.

The fractional change in nonlinear ultrasonic parameter is related to the stress and dislocation density (Ref 30, 31) by equation,

$$\frac{\Delta\beta}{\beta_0} \propto \sigma\Lambda L^4 \quad (\text{Eq 16})$$

where  $L$  is the dislocation loop length and  $\sigma$  is the stress.

Hence from Eq 15 and 16, we have

$$\frac{\Delta\beta}{\beta_0} \propto V_f^{1/2} r_a^{1/2} \Lambda L^4 \quad (\text{Eq 17})$$

Equation 17 clearly depicts that the volume fraction and radius of precipitates will cause a change in NLU parameter,  $\beta$ .

The results of the NLU measurement in the present study show a significant increase in the NLU parameter when the precipitate size is around 250 nm and beyond. From Fig. 11 it was observed that among the three different types of precipitates, growth of Laves phase precipitates is quite significant and the size of Laves phase is in the range of 200 nm and beyond after 4% of strain. This is in agreement with the literature data. Generally, Laves phases are coherent in nature when they generate but become incoherent when the radius ( $r_a$ ) exceeds a critical value ( $r_a > r_{\text{acritical}}$ ) (Ref 7, 30). The variation of NLU parameter also follows the same trend as the strain hardening and strength coefficient with strain% (Fig. 14). From the microstructural and mechanical behavior study, the following interpretations can be made: increase in the NLU parameter till 6% of strain is due to the increase in the volume fraction and the size of precipitates within the coherency limit. Beyond 6% strain, the coherency of precipitates is lost, the misfit is large enough to create space between the dislocation and interface array equals to the lattice spacing. Hence at this stage the local stress caused by the precipitates becomes almost zero (Eq 15). As a result, NLU parameter drops drastically.

## 6. Conclusion

This paper describes the effect of generation and growth of precipitates and voids on the nonlinear ultrasonic parameter during creep in P92 steel, an important material for headers and

pipings of power plants. It is well known that the fine precipitates are responsible for high creep strength in P92 steel. With longer exposure at high temperature, along with the coarsening of the existing precipitates ( $M_{23}C_6$  & MX), a new phase called Laves phase appears. Laves phase not only reduces the creep strength, but also triggers cavity formation. Identification of strain% at which formation of Laves phase takes place can help to assess the remaining life of components made of P92 steel.

This study aimed to find the applicability of non-invasive NLU technique to identify the onset of mechanical strength deterioration due to the formation and growth of Laves phase in P92 steel. Field applicable, pulse-echo based nonlinear ultrasonic technique (PENLU) in two different test modes; multiple samples single interruption (MSSI) and single sample multiple interruptions (SSMI) were used for this study.

In both the test modes, it was established that in P92 steel, the growth of Laves phase beyond the coherency limit, can be detected by monitoring NLU parameter over a period of time. It is concluded that a peak in the variation of NLU parameter with the creep strain% corresponds to the onset of deterioration of mechanical strength.

## Acknowledgments

Authors are grateful to the Director, CSIR-National Metallurgical Laboratory, Jamshedpur for his kind permission to publish this work. The first author also acknowledges the financial support from the Council of Scientific and Industrial Research (CSIR), India.

## References

1. Y. Wang, K.H. Mayer, A. Scholz, C. Berger, H. Chilukuru, K. Durst and W. Blum, Development of New 11% Cr Heat Resistant Ferritic Steels with Enhanced Creep Resistance for Steam Power Plants with Operating Steam Temperatures up to 650 C, *Mater. Sci. Eng. A*, 2009, **510**, p 180–184
2. V. Skorobogatikh, I. Schenkova, V. Dudko, A. Belyakov, and R. Kaibyshev, Microstructure Evolution in a 9% Cr Heat Resistant Steel During Creep Tests, in *Materials Science Forum*, vol 638 (Trans Tech Publications, 2010), pp. 2315–2320
3. F. Abe, Long-Term Stabilization of Creep-Resistant Ferritic Steels for Highly Efficient Ultra-Supercritical Power Plants, in *Advances in Science and Technology*, vol 72 (Trans Tech Publications, 2010), pp. 12–21
4. K.H. Mayer, A. Scholz and Y. Wang, Investigations of Ferritic/Martensitic Super Heat Resistant 11–12% Cr Steels for 650 °C Power Plants, *Mater. Wiss. Werkst.*, 2006, **37**(10), p 806–811
5. Y. Hasegawa, M. Ohgami and T. Murahi, Grain Boundary Strengthening Mechanism of Tungsten Containing 9 to 12% Chromium Ferritic Heat Resistant Steels at 650 deg C, *J. Soc. Mater. Sci. Jpn.*, 2003, **52**(7), p 843–850
6. D. Rojas, J. Garcia, O. Prat, G. Sauthoff and A.R. Kaysser-Pyzalla, 9% Cr Heat Resistant Steels: Alloy Design, Microstructure Evolution and Creep Response at 650 C, *Mater. Sci. Eng. A*, 2011, **528**(15), p 5164–5176
7. K. Miyahara, J.H. Hwang and Y. Shimode, Aging Phenomena Before the Precipitation of the Bulky Laves Phase in Fe-10% Cr Ferritic Alloys, *Scr. Metall. Mater.*, 1995, **32**(12), p 1917–1921
8. J. Hald, Metallurgy and Creep Properties of new 9–12% Cr Steels, *Steel Res. Int.*, 1996, **67**(9), p 369–374
9. A. Kostka, K.G. Tak, R.J. Hellmig, Y. Estrin and G. Eggeler, On the Contribution of Carbides and Micrograin Boundaries to the creep Strength of Tempered Martensite Ferritic Steels, *Acta Mater.*, 2007, **55**(2), p 539–550
10. B. Raj, B.K. Choudhary and R.S. Raman, Mechanical Properties and Non-destructive Evaluation of Chromium–Molybdenum Ferritic Steels for Steam Generator Application, *Int. J. Press. Vessels Pip.*, 2004, **81**(6), p 521–534
11. Z.J. Chen, M.R. Govindaraju, D.C. Jiles, S.B. Biner and M.J. Sablik, Assessment of Creep Damage of Ferromagnetic Material Using Magnetic Inspection, *IEEE Trans. Magn.*, 1994, **30**(6), p 4596–4598
12. H. Willems, T. Jayakumar, T. Koble, and W. Theiner, in *Proceedings of the 2nd annual report on project D4, Cost 501/II WP 5C, European Committee on Special Testing, Izfp Saarbrucken* (1990)
13. H. Carreon, Detection of Creep Damage in a Nickel-Based Superalloy Turbine Bucket Using Eddy Current Imaging, *Nondest. Test. Eval.*, 2009, **24**(1–2), p 233–241
14. A. Saxena, Electrical Potential Technique for Monitoring Subcritical Crack Growth at Elevated Temperatures, *Eng. Fract. Mech.*, 1980, **13**(4), p 741–750
15. F. Masuyama, Creep Degradation in Welds of Mod. 9Cr-1Mo Steel, *Int. J. Press. Vessels Pip.*, 2006, **83**(11–12), p 819–825
16. S. Kirihara, M. Shiga, M. Sukekawa, T. Yoshioka and C. Asano, Fundamental Study on Non-Destructive Detection of Creep Damage for Low Alloy Steel, *J. Soc. Mater. Sci. Jpn.*, 1984, **33**(371), p 1097–1102
17. B.J. Cane, Remaining Creep Life Estimation by Strain Assessment on Plant, *Int. J. Press. Vessels Pip.*, 1982, **10**(1), p 11–30
18. A. Pyzalla, B. Camin, T. Buslaps, M. Di Michiel, H. Kaminski, A. Kottar, A. Pernack and W. Reimers, Simultaneous Tomography and Diffraction Analysis of Creep Damage, *Science*, 2005, **308**(5718), p 92–95
19. X. Wang, X. Wang, X.G. Niu, D.M. Xiao and X.L. Hu, Application of Nonlinear Ultrasonic Technique to Characterize the Creep Damage in ASME T92 Steel Welded Joints, *NDT and E Int.*, 2018, **98**, p 8–16
20. T. Ohtani, H. Ogi and M. Hirao, Noncontact Evaluation of Surface-Wave Nonlinearity for Creep Damage in Cr–Mo–V Steel, *Jpn. J. Appl. Phys.*, 2009, **48**(7S), p 07GD02
21. S. Baby, B.N. Kowmudi, C.M. Om Prakash, D.V.V. Satyanarayana, K. Balasubramaniam and V. Kumar, Creep damage assessment in titanium alloy using a nonlinear ultrasonic technique, *Scr. Mater.*, 2008, **59**(8), p 818–821
22. J.S. Valluri, K. Balasubramaniam and R.V. Prakash, Creep Damage Characterization Using Non-linear Ultrasonic Techniques, *Acta Mater.*, 2010, **58**(6), p 2079–2090
23. C. Kim, Creep Damage Characterization of Ni-Based Super Alloy by Acoustic Nonlinearity, *Prog. Nat. Sci. Mater. Int.*, 2012, **22**(4), p 303–310
24. J. Park, M. Kim, B. Chi and C. Jang, Correlation of Metallurgical Analysis & Higher Harmonic Ultrasound Response for Long Term Isothermally Aged and Crept FM Steel for USC TPP Turbine Rotors, *NDT E Int.*, 2013, **54**, p 159–165
25. J. Kang, J. Qu, A. Saxena, and I. Jacobs, On the Detection of Creep Damage in a Directionally Solidified Nickel Base Superalloy Using Nonlinear Ultrasound, in *AIP Conference Proceedings*, vol 700, no 1 (2004), pp. 1248–1255
26. Y. Xiang, M. Deng and F.Z. Xuan, Creep Damage Characterization Using Nonlinear Ultrasonic Guided Wave Method: A Mesoscale Model, *J. Appl. Phys.*, 2014, **115**(4), p 044914
27. K.Y. Jhang, Nonlinear Ultrasonic Techniques for Non-destructive Assessment of Micro Damage in Material: A Review, *Int. J. Precis. Eng. Manuf.*, 2009, **10**(1), p 123–135
28. A.N. Norris, in *Nonlinear Acoustics*, ed. M. Hamilton, D. Blackstock (Academic Press, San Diego, CA, 1998), pp. 263–264
29. D.C. Wallace, Thermoelasticity of Stressed Materials and Comparison of Various Elastic Constants, *Phys. Rev.*, 1967, **162**(3), p 776
30. J.H. Cantrell, Crystalline Structure and Symmetry Dependence of Acoustic Nonlinearity Parameters, *J. Appl. Phys.*, 1994, **76**(6), p 3372–3380
31. J. Melngailis, A.A. Maradudin and A. Seeger, Diffraction of Light by Ultrasound in Anharmonic Crystals, *Phys. Rev.*, 1963, **131**(5), p 1972
32. M.D. Mathew, K.L. Murty, K.B.S. Rao and S.L. Mannan, Ball Indentation Studies on the Effect of Aging on Mechanical Behaviour of Alloy 625, *Mater. Sci. Eng. A*, 1999, **264**(1), p 159–166
33. G. Das, S. Ghosh and S.K. Sahay, Use of Ball Indentation Technique to Determine the Change of Tensile Properties of SS316L Steel Due to Cold Rolling, *Mater. Lett.*, 2005, **59**(18), p 2246–2251

34. V. Karthik, P. Visweswaran, A. Bhushan, D.N. Pawaskar, K.V. Kasiviswanathan, T. Jayakumar and B. Raj, Finite Element Analysis of Spherical Indentation to Study Pile-Up/Sink-In Phenomena in Steels and Experimental Validation, *Int. J. Mech. Sci.*, 2012, **54**(1), p 74–83
35. A. Metya, M. Ghosh, N. Parida and S.P. Sagar, Higher Harmonic Analysis of Ultrasonic Signal for Ageing Behaviour Study of C-250 Grade Maraging Steel, *NDT E Int.*, 2008, **41**(6), p 484–489

**Publisher's Note** Springer Nature remains neutral with regard to jurisdictional claims in published maps and institutional affiliations.